JSS FOCUS ISSUE ON DEFECT CHARACTERIZATION IN SEMICONDUCTOR MATERIALS AND DEVICES

Defects and Dopants in Silicon Nanowires Produced by Metal-Assisted Chemical Etching

M. Fanciulli,[a,b,*,z] M. Belli,[b] S. Paleari,[a] A. Lamperti,[b] M. Sironi,[a] and A. Pizio[a]

[a]Department of Materials Science, University of Milano Bicocca, Milano 20125, Italy
[b]Laboratorio MDM, IMM-CNR, 20864 Agrate Brianza (MB), Italy

The current status of the investigation of defects in silicon nanowires and at the interface between Si and its oxide in 1D nanostructures is reviewed and discussed. The paper concentrates on nanowires produced by metal assisted chemical etching. The role of defects at the interface between the semiconductor and its oxide and of hydrogen in passivating donor atoms is addressed.
© The Author(s) 2016. Published by ECS. This is an open access article distributed under the terms of the Creative Commons Attribution Non-Commercial No Derivatives 4.0 License (CC BY-NC-ND, http://creativecommons.org/licenses/by-nc-nd/4.0/), which permits non-commercial reuse, distribution, and reproduction in any medium, provided the original work is not changed in any way and is properly cited. For permission for commercial reuse, please email: oa@electrochem.org. [DOI: 10.1149/2.0171604jss] All rights reserved.

Manuscript submitted November 18, 2015; revised manuscript received December 15, 2015. Published January 22, 2016. This was Paper 819 presented at the Phoenix, Arizona, Meeting of the Society, October 11–15, 2015. *This paper is part of the JSS Focus Issue on Defect Characterization in Semiconductor Materials and Devices.*

Several architectures for ultra-scaled devices targeting classical and quantum information processing, chemical sensing, and energy harvesting and production rely on silicon and germanium nanowires (SiNWs, GeNWs).[1–7] Despite the efforts in the preparation and characterization of these nanostructures, some fundamental issues remain relatively unexplored. In particular the investigation of defects in 1D nanostructures at the interface between the semiconductor and its oxide or other semiconductors or oxides in core-shell structures represents an important challenge, as the NW diameter reduces and the surface-to-volume ratio increases.[8,9] NWs represent also an interesting system to investigate more fundamental issues such as, for example, Mott transition, spin relaxation mechanisms and scattering processes. In this paper we will review the current experimental data and understanding of the n-type doping of silicon nanowires produced by Metal-assisted Chemical Etching (MACE). The main results concerning the investigation of defects in SiNWs are related to the observation of defects at the Si/SiO_2 interface and in the SiO_2[10–16] and to donors.[12,13,16,17] The role of hydrogen and defects at the interface between the semiconductor and its oxide in the donor de-activation mechanisms will be discussed. Data on SiNWs with diameters larger than 20 nm will be reported therefore excluding discussion of dielectric mismatch and quantum confinement effects.

Experimental

Nanowires fabrication.—SiNWs were prepared according to the procedure described by Zhang et al.[18] Either highly resistive ($\rho > 5000\ \Omega$ cm) silicon (100) wafers or silicon (100) p-type wafers ($\rho = 8$–$12\ \Omega$ cm) with a 10 μm thick epilayer on top, n-type (phosphorus doped) with dopant concentration of $N_D = 1 \times 10^{17}$ cm^{-3} have been used (with the exception of the sample for ToF-SIMS investigation, which was characterized by an epilayer thickness of 5 μm and a P concentration of $N_D = 1 \times 10^{19}$ cm^{-3}). Samples having an area of 2×2 cm^2 were cleaned with a piranha solution (H_2SO_4/H_2O_2 3:1 v/v) for 10 min at room temperature to entirely remove organics. Wafers were then rinsed with water, etched with a 4.8% HF aqueous solution for 3 min at room temperature, immediately placed into an Ag coating solution containing 4.6 M HF and 0.005 M $AgNO_3$ for 1 min for electroless deposition of Ag nanoparticles, washed with water to remove the extra Ag^+ ions and then immersed in the etchant solution composed of 4.8 M HF and H_2O_2 0.4 M for 4 min at room temperature. Samples were then washed with water, immersed in dilute HNO_3 (1:1 v/v) to remove residual Ag nanoparticles, washed first with water, then with isopropyl alcohol, then they were left to dry in air. The samples were then finally cut to dimensions suitable for characterization (3×12 mm^2). Further annealing steps, aiming at the investigation of the defects evolution, were performed in a rapid thermal annealing system or in a horizontal furnace, in N_2 and at different temperatures in the range 60°C- 600°C. After each annealing step the samples were either left for 28 hours in air to maximize the P_b center signal or the increasing of the signal was followed as discussed later on.

Characterization.—The SiNWs have been characterized by a variety of methods to access their morphology, their chemical properties, and to address defects and dopants. Morphological characterization was performed with Scanning Electron Microscopy (SEM, Zeiss SUPRA 40), chemical properties were investigated with Time-of-Flight Secondary Ion Mass Spectrometry (ToF-SIMS, ION-TOF IV) and X-ray Photoelectron Spectroscopy (XPS, PHI 5600). ToF-SIMS mass spectra were acquired using a 25 keV Ga^+ ion beam with few pA current over a 50 μm × 50 μm area for analysis and 1 keV Cs^+ ion beam with nA current for raster sputtering over an area of 300 μm × 300 μm, in negative polarity and interlaced mode; secondary ions are collected in time-of-flight spectrometer granting a mass resolution of at least 7000 at the investigated masses. The analysis has been stopped after about 200 nm depth sputtering from the surface (calibrated from a SiO_2 reference sample). XPS measurements were acquired using a monochromatic Al K_α X-ray source (1486.6 eV) with pass energy 5.85 eV over a mm^2 area; the instrument resolution is 0.1 eV. XPS spectra were fitted using XPSPEAK4.1 software, considering Shirley background, doublets for Si 2p peak with spin orbit splitting of 0.59, and pseudo-Voigt functions. Positions of the lines are calibrated against the C 1s line descending from adventitious carbon. The chemical environment at the surface of the NWs was investigated by Fourier Transform Infrared spectroscopy (FT-IR) using a Jasco FT/IR Michelson interferometer, in the wavenumber range 4000–400 cm^{-1} with 0.25 cm^{-1} resolution. Absorbance spectra were measured at room temperature, using a double stage rotary pump to evacuate the sample chamber. Dual beam measurement mode was operated by acquiring a reference spectrum without the sample (I_0) as reference, then calculating sample absorbance (A) according to $A = \mathrm{Log}(I_0/I)$. Electron Paramagnetic Resonance spectroscopy (EPR) has been carried out in an X band (9.4 GHz) spectrometer equipped with a high Q-factor cylindrical cavity (Bruker EF4122sHQ). A frequency counter was used to monitor the microwave frequency. The g-factors and absolute spectral intensities were determined using the reference signal of a standard Bruker marker

*Electrochemical Society Active Member.
zE-mail: marco.fanciulli@unimib.it

Downloaded on 2018-07-20 to IP 207.241.231.81 address. Redistribution subject to ECS terms of use (see ecsdl.org/site/terms_use) unless CC License in place (see abstract).

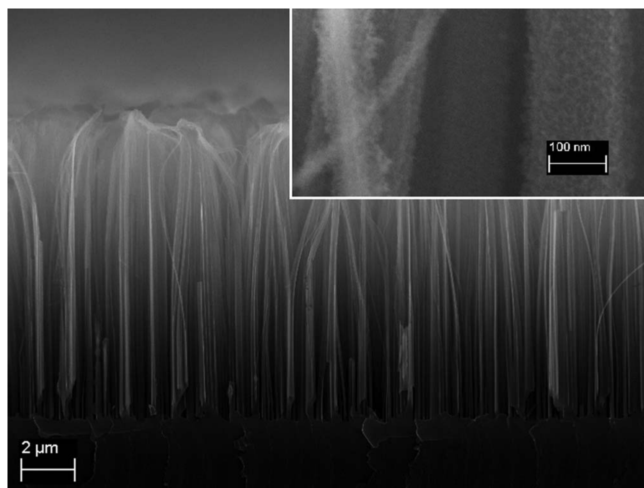

Figure 1. SEM micrograph cross section view of typical intrinsic SiNWs produced by MACE, showing vertically aligned wires and a flat etch profile. The nanowires are 11.3 μm tall, and display diameters in the range 25 – 200 nm, with an approximate average diameter of 60 nm. Inset: detail at high magnification showing the porosity at the surface of some relatively large nanowires.

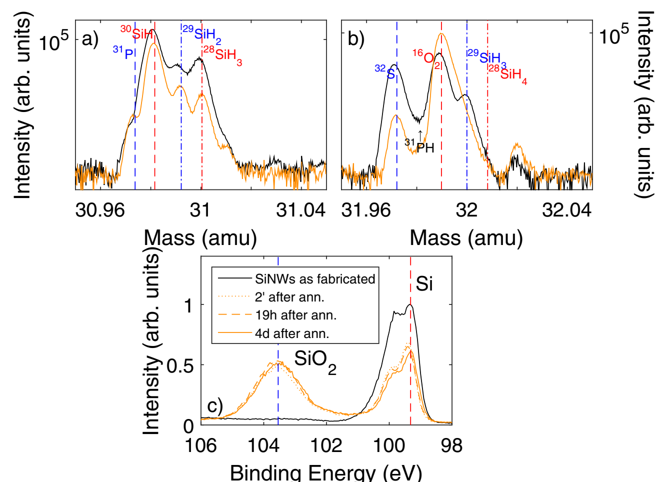

Figure 2. a), b) ToF-SIMS mass spectra for as-fabricated phosphorus-doped SiNWs at nominal mass m = 31 amu and m = 32 amu and for the same sample long time after a high temperature annealing and the following air exposure. Note the decrease in the contribution from SiH-related ions. c) XPS of the Si 2p core level: contributions from Si^0 and SiH are well evident in as fabricated sample (increased shoulder on left side of Si peak), while after treatment and air exposure silicon oxide components emerge, SiO_2 in particular.

characterized by g factor g = 1.97984(1).[19] The samples were tied onto a quartz rod with teflon tape and inserted into a flow-cryostat capable of operating at temperatures in the range 4 K – 300 K.

Experimental Results and Discussion

In Fig. 1 the morphology of the SiNWs produced by MACE is shown in a representative SEM micrograph. These images show vertically aligned porous NWs with diameters in the range 25–200 nm and an average diameter of ~60 nm, as reported in Table I. The nanowires height, 11.3 μm in the example of Fig. 1, can be tuned by adjusting the etch time and the concentrations of etching solution components. Morphological parameters were essentially unaffected by the thermal treatments in the adopted conditions.

ToF-SIMS mass spectra at nominal mass m = 31 amu and m = 32 amu are shown in Fig. 2a and Fig. 2b respectively. At mass m = 31 amu (Fig. 2a) we can distinguish the presence of at least 4 contributions from different ions and, in particular, from lower to higher mass ^{31}P, ^{30}SiH, $^{29}SiH_2$ and $^{28}SiH_3$.[20,21] The intensity of SiH-related masses denotes the high contribution from Si-H bonds in the as-prepared nanowires. The peak related with P can be hardly seen as a shoulder in the tail of the ^{30}SiH contribution, not fully de-convoluted from the ^{30}SiH mass contribution. It is worth noticing that the chosen measurement setup is capable of granting full peak separation (i.e. mass resolution) between P and ^{30}SiH on flat P-doped wafer. Here the observed overlapping underlines the high contribution from SiH-related ions. Looking at mass m = 32 amu we have a further confirmation of SiH ion abundance, as can be seen from the clear detection of contributions from $^{30}SiH_2$, $^{29}SiH_3$ and $^{28}SiH_4$ ions.[20,21] Further, here we observe a contribution from sulfur and oxygen (seen as molecular O_2 ion). To further elucidate the chemistry of as-prepared NWs, with a particular attention to the surface and sub-surface regions, we performed XPS measurements across the Si 2p spectral region (Fig. 2c). From the fitting we could resolve the major contribution originating from Si^0 chemical state and the presence of minor contribution from SiO and SiO_2 oxide states. The presence of the sub-oxidation contribution is probably due to the short exposure in air while transferring the sample from the clean room to the (ex-situ) XPS analysis chamber. Further, the fitting is well matched only when also considering a contribution at 99.6 eV associated with SiH bond.[22,23]

Table I. Samples properties. Average diameters extracted from Scanning Electron Microscopy micrographs reflect the statistical data of an ensemble of some tens of nanowires. Doping in SiNWs determined by Hall effect on the virgin epilayer.

Sample	Average Diameter [nm]	Doping [atoms/cm^{-3}]
SiNWs-i	60 ± 40	-
SiNWs-n	70 ± 30	P, 10^{17}

FT-IR data are reported in Fig. 3 for different treatments. A reference sample is plotted against the as-prepared SiNWs to reveal the

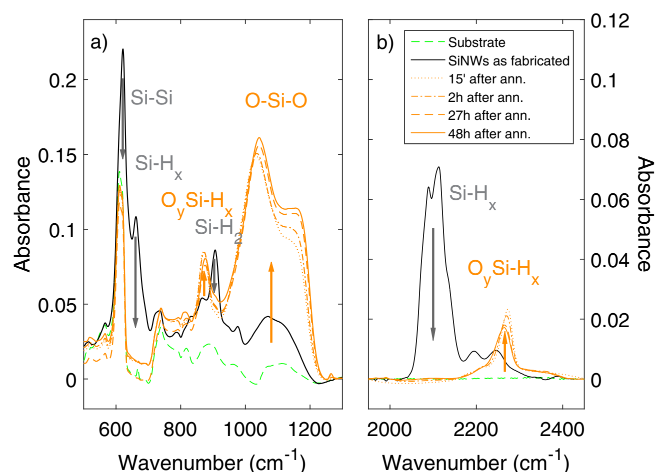

Figure 3. FT-IR absorbance spectra recorded in dual beam mode: reference flat substrate showing the Si-Si mode (dashed green); after MACE process (blue) $Si\text{-}H_x$ signals appear (peaks at 625, 666, 910, 2196, 2250, 2273 cm^{-1}), prevailing over the O_ySiH_x (876, 2196, 2250, 2273 cm^{-1}); the spectrum recorded just 15 minutes after the annealing (550°C 15 min.) showed a drop in the Si-H peaks and an increase in those related to O_ySiH_x. Signals of the SiO_x vibrational mode in the spectral region 1065 - 1173 cm^{-1} of the sample before the annealing are negligible with respect to the sample after annealing (dotted red). The evolution in the first 48 hours is also reported for the sake of completeness, but does not show any major changes Resolution is reduced to 2 cm^{-1} to suppress the thin film interference pattern due to internal reflections in the substrate.

Downloaded on 2018-07-20 to IP 207.241.231.81 address. Redistribution subject to ECS terms of use (see ecsdl.org/site/terms_use) unless CC License in place (see abstract).

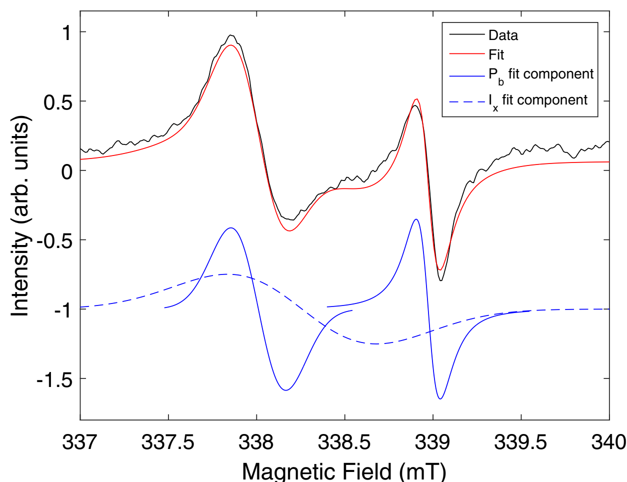

Figure 4. EPR spectrum (RT, H||[111]) after air exposure (t>20 h): the fit (solid red, with individual components in blue depicted as shifted below the experimental data) evidences two P_b peaks, as expected by symmetry considerations when the magnetic field is oriented along one of the [111] directions of the Si crystal. A third component representing the I_x defect is indicated by the dashed blue line.

prevalence of Si-H bonds (Si-H_x peaks located at 625, 666, 910, 2087, 2110, 2141 cm^{-1}) and the limited contribution of O_ySi-H_x shoulders (876, 2196, 2250, 2273 cm^{-1}).[24,25] Almost no oxidation at the surface of nanowires can be inferred from the absence of the typical infrared absorption bands of the Si_xO_y vibrational modes in the region 1065 - 1176 cm^{-1}. Additional spectra, recorded from 15 minutes up to 48 hours after the annealing, show a drop in the Si-H peaks and an increase of the Si_yO_x and O_ySiH_x modes. The brief exposure to air after the thermal treatment is sufficient to oxidize the NWs surface, as observed in the XPS measurements, and then only minor evolution occurs.

Electron paramagnetic resonance of the as prepared intrinsic SiNWs does not show any resonance, while the n-type SiNWs show the hyperfine splitted resonance of substitutional P.[26] Upon annealing and exposure to air the signals of the well-known P_b center[27–29] appear in both samples, while the P doublet first increases and, when the P_b signal appears, starts to decrease as reported in Fig. 5d. A further, broad signal is always present along with the P_b signal (Fig. 4). It is characterized by a g factor of 2.0052(8), and a Voigtian peak-to-peak width of 0.84(1) mT. The signal is isotropic with an isotropic linewidth. We can tentatively attribute the signal to the I_x center.[30] A full understanding of the nature of this signal is still missing. Previous investigations reported a g-factor variability between g = 2.0047 and g = 2.0050, a large width which is comparable to our results, and the identification of this signal as related to a center at the interface between Si and SiO_2. We do not intend to focus on such a defect, though we here add to the discussion that it presents a time evolution of the intensity upon exposure to air similar to P_b, but slightly faster (Figure 5a). The example reported in the figure evidences a characteristic exponential increase for the I_x intensity τ_{Ix} of ∼ 5 hours, while, for the same sample, the P_b signal increases, with a characteristic time constant τ_{Pb} of ∼ 9 hours. Upon saturation the I_x intensity is between 25% and 65% of the P_b intensity a result that depends on the specific sample analyzed. The time evolution of the P_b and I_x signals depend strongly on the temperature and humidity of the air during the exposure.

Upon annealing of doped SiNWs in N_2 in the temperature range 60–300°C, EPR reveals the increase of the P^0 resonance. This result is attributed to the dissociation of PH complexes formed during the MACE process

$$(PH)^0 \rightarrow P^+ + H^- \quad [1]$$

The dissociation, observed upon isothermal annealing, is consistent with the first-order rate law kinetics observed in porous silicon

$$I(t) = I_0\left(1 - e^{-kt}\right) \quad [2]$$

$$k = k_0 e^{-E_a/k_B T} \quad [3]$$

with values of the constants $k_0 = 6 \times 10^{13}\ s^{-1}$; $E_a = 1.2$ eV reported in literature[31–33] (see Fig. 5b). Donor passivation by hydrogen has been extensively studied for P-doped bulk (nanoporous) Si.[31–34] First-principles pseudopotential-density functional calculations revealed that H is located on the extension of a P-Si bond on the Si side, with the Si-H pair relaxing away from P, leaving the P atom threefold coordinated.[35,36] The electronic level scheme of acceptors and donors in silicon nanowires produced by the VLS method has been recently investigated by Sato and coworkers using deep level transient spectroscopy and photon-induced current transient spectroscopy.[37] For n-type SiNWs they reported four levels in the gap. In particular the E2 (with 0.25 eV activation energy) was not assigned to any specific

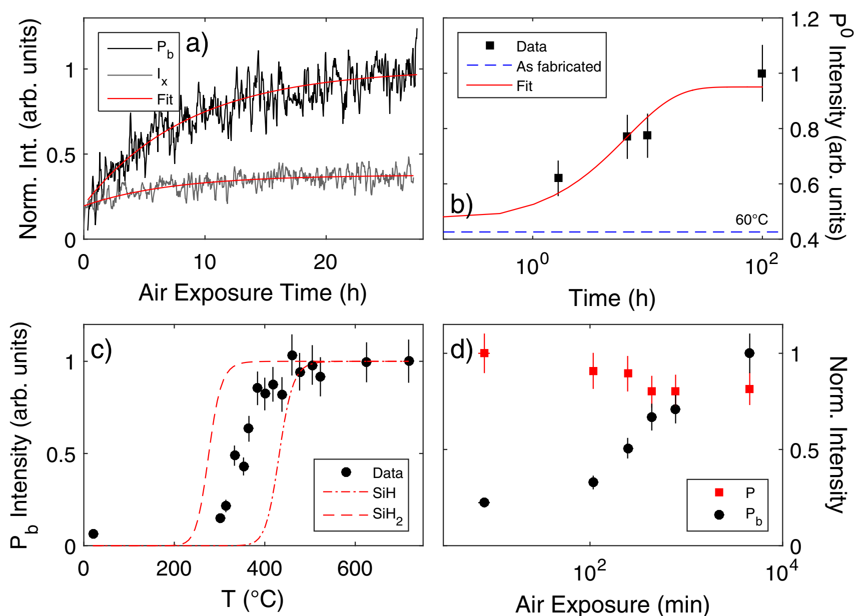

Figure 5. a) Time evolution of the intensity of the EPR signals due to P_b (black) and I_x centers (gray) following an annealing step at T = 365°C for 60 min. Red lines are fittings to the data with the model explained in the text. After annealing, the sample was left at room temperature in N_2 for 18 hours, and then exposed to air. The EPR spectrum of the annealed sample did not reveal any signal and was not affected by the long exposure time to an inert atmosphere. The P_b signals begin to increase only after exposure to air. The maximum intensity is determined by the annealing temperature. b) Intensity of the P^0 peaks upon isothermal annealing at T = 60°C. Data are consistent with the dissociation kinetics of PH complexes described by Eq. 2.[34–36] c) Maximal P_b intensity after isochronal anneal (t = 1 h). In the figure the dissociation of SiH and SiH_2 is reported for comparison. d) Intensity of the P_b and P^0 centers as function of exposure to air after an annealing step.

Downloaded on 2018-07-20 to IP 207.241.231.81 address. Redistribution subject to ECS terms of use (see ecsdl.org/site/terms_use) unless CC License in place (see abstract).

defect, while the E2B (with 0.26 eV activation energy) was associated with the E-center (P-V complex). We did not observe, by EPR signals, which could be attributed to the P-V complex. This result is not conclusive and additional work is necessary to clarify it. However, we tentatively suggest that the E2 level is related to complexes involving H.

ToF-SIMS, XPS (Fig. 2) and FT-IR (Fig. 3) investigation of intrinsic or doped SiNWs annealed at temperatures higher than 300°C show: i) a decrease of the SiH_x signals; ii) an increase of the SiO_x signals. These results indicate hydrogen release from the SiNWs and a progressive oxidation. The latter strongly depends on the air exposure time after the annealing steps. Immediately after each annealing step EPR shows a very weak signal related to the presence of dangling bonds at the interface (P_b centers) between the SiNW and the growing SiO_x layer. The P_b signal increases as function of exposure to air at room temperature with a time constant of the order of 9 hours as shown in Fig. 5a. The EPR spectrum is not affected by long settling time in inert environment, the P_b signal begins to increase only after exposure to air, as we verified in one case by leaving the sample at room temperature for 18 h in N_2.

It is possible to indirectly investigate the dissociation kinetics of the Si-H bonds by recording the increase of the maximum P_b signal observed by EPR after each annealing step followed by 28 h exposure to air at room temperature. As a first-order approximation, the trend can be interpreted as an exponential recovery:

$$I = I_\infty \left(1 - e^{(t-t_0)/\tau}\right) \quad [4]$$

with maximum intensity I_∞ dependent on annealing temperature (T) and time (t). Such a functional form is consistent with second order dissociation kinetics:

$$I_\infty = \frac{1}{1 + Ckt} \quad [5]$$

$$k = \nu_0 e^{-E_a/k_B T} \quad [6]$$

with $\nu_0 = 120$ cm^2 s (fixed) and $E_a = 2.39 \pm 0.02$ eV. The activation energy is an intermediate value between those found for the dissociation of the SiH and SiH_2 centers as reported in Fig. 5c for crystalline silicon flat surface.[38] However such a model is only indicative as a simplified approximation and a thorough investigation is necessary to address the details of the dissociation kinetics. For example, the same intensity trend may be obtained by considering a distribution of activation energies and/or of the pre-exponential factor. Nevertheless, the steep slope of the P_b intensity upon isochronal annealing allows to exclude any first order process as the origin of P_b signal increase. In such a case a smoother slope is expected, even in the absence of a distribution of the relevant parameters.

It is interesting to note that XPS and FT-IR show the oxidation of silicon well before the occurrence in the EPR spectrum of the P_b-related signals. The silicon oxide should go through small rearrangements not evidently visible with XPS or FT-IR leading eventually to the interfacial defects formation.

The average diameter of the SiNWs is larger than the value below which quantum confinement and dielectric mismatch effects should be observed. However, the SiNWs system allows a detailed and controlled investigation, using EPR, of the depletion region formation due to interface defects, since the P_b center concentration can be modified by annealing followed by exposure to air. Fig. 5d reports the intensity of the P and P_b signals after an initial annealing step followed by exposure to air. The intensities of the P and of the P_b, determined against the marker, have been measured at 15 K and at RT respectively to avoid saturation effects. As expected an increase of the P_b centers results in a decrease of the P signal.

Conclusions

SiNWs produced by the MACE method have been investigated by electron spin resonance spectroscopy to investigate defects and dopants, and by complementary techniques (SEM, TEM, XPS, ToF-SIMS, FT-IR) to determine the morphological and chemical properties. The nanowires, in addition to their interest stemming from the different applications, represent also a model system in which several intriguing phenomena may be investigated. In SiNWs we have shown how H is terminating the nanowire surface preventing its oxidation and the passivating of donors. Upon thermal treatments and exposure to air the nanowires go through a series of chemical reactions leading to the dissociation of PH complexes, H desorption, oxidation, formation of defects at the interface between Si and SiO_2, the P_b centers, which leads to the formation of a depletion region deactivating a fraction of the donors. Due to the average size of the investigated SiNWs, quantum confinement or dielectric mismatch effects have not been detected by EPR.

Acknowledgments

We thank Prof. S. Binetti at the University of Milano Bicocca for her assistance in the FT-IR measurements.

References

1. P. Yang, R. Yan, and M. Fardy, *Nano Lett.* **10**, 1529 (2010).
2. Y. Huang and K-N. Tu, *Silicon and Silicide Nanowires: Applications, Fabrication, and Properties*, CRC Press (2013).
3. M. Hasan, M. F. Huq, and Z. H. Mahmood, *SpringerPlus* **2**, 151 (2013).
4. K-Q. Penga, X. Wanga, L. Lia, Y. Hua, and S-T. Leeb, *Nano Today* **8**, 75 (2013).
5. S. T. Picraux, S. A. Dayeh, P. Manandhar, D. E. Perea, and S. G. Choi, *JOM* **62**, 35 (2010).
6. L. Z. Pei and Z. Y. Cai, *Recent Patents on Nanotechnology* **6**, 44 (2012).
7. N. K. Mahenderkar, Y-C. Liu, J. A. Koza, and J. A. Switzer, *Nanotechnology* **26**, 195705 (2015).
8. V. Schmidt, S. Senz, and U. Gösele, *Appl. Phys. A.* **86**, 187 (2007).
9. M. T. Björk, H. Schmid, J. Knoch, H. Riel, and W. Riess, *Nature Nanotech.* **4**, 103 (2009).
10. A. Baumer, M. Stutzmann, M. S. Brandt, F. C. K. Au, and S. T. Lee, *App. Phys. Lett.* **85**, 43 (2004).
11. R. P. Wang, *Appl. Phys. Lett.* **88**, 142104 (2006).
12. M. Fanciulli, A. Vellei, C. Canevali, S. Baldovino, G. Pennelli, and M. Longo, *Nanosci. Nanotechnol. Lett.* **3**, 568 (2011).
13. M. Fanciulli, A. Molle, S. Baldovino, and A. Vellei, *Microelectronic Engineering* **88**, 1482 (2011).
14. M. Jivanescu, A. Stesmans, R. Kurstjens, and F. Dross, *Appl. Phys. Lett.* **100**, 082110 (2012).
15. K. Yin, Y. Zhao, X. Wang, L. Liu, G. Xue, S-T. Lee, and M. Shao, *App. Phys. Lett.* **104**, 033110 (2014).
16. N. Fukata, S. Ishida, S. Yokono, R. Takiguchi, J. Chen, T. Sekiguchi, and K. Murakami, *Nano Lett.* **11**, 651 (2011).
17. M. Fanciulli, M. Belli, S. Paleari, A. Lamperti, A. Molle, M. Sironi, and A. Pizio, *ECS Transactions*, **69**(5) 69 (2015).
18. M. Zhang, K. Peng, X. Fan, J. Jie, R. Zhang, S. Lee, and N. Wong, *J. Phys. Chem. C* **112**, 4444 (2008).
19. Bruker EPR Chromium marker.
20. G. Audi and A. H. Wapstra, *Nucl. Phys. A* **565**, 1 (1993).
21. G. Audi and A. H. Wapstra, *Nucl. Phys. A* **595**, 409 (1995).
22. A. Thøgersen, J. H. Selj, and E. S. Marstein, *J. Electrochem. Soc.* **159**, D276 (2012).
23. M. Y. Bashouti, K. Sardashti, J. Ristein, and S. Christiansen, *Nanoscale Research Letters* **8**, 41 (2013); M. Y. Bashouti, M. Pietsch, K. Sardashti, G. Brönstrup, S. W. Schmitt, S. K. Srivastava, J. Ristein, J. Arbiol, H. Haick, and S. Christiansen, *Hybrid Silicon Nanowires: From Basic Research to Applied Nanotechnology*, in Nanowires: Recent Advances edited by X. Peng, ISBN 978-953-51-0898-6, Published 19 December 2012 under CC BY 3.0 license, by INFOTECH, Chapter 9, pp.177. doi:10.5772/54383.
24. D. B. Mawhinney, J. A. Glass, and J. T. Yates, *J. Phys. Chem. B* **101**, 1202 (1997).
25. X. H. Sun, S. D. Wang, N. B. Wong, D. D. D. Ma, S. T. Lee, and B. K. Teo, *Inorg. Chem.* **42**, 2398 (2003).
26. G. Feher, *Phys. Rev.* **114**, 1219 (1959).
27. P. J. Caplan, E. H. Pointdexter, B. Deal, and R. R. Razouk, *J. Appl. Phys.* **50**, 5847 (1979).
28. A. Stesmans and V. Afanasev, *J. Appl. Phys.* **83**, 2449 (1998).
29. K. L. Brower, *Semicond. Sci. Technol.* **4**, 970 (1989).
30. K. Keunen, A. Stesmans, and V. V. Afanas'ev, *Phys. Rev. B* **84**, 085329 (2011).
31. K. Bergman, M. Stavola, S. J. Pearton, and J. Lopata, *Phys. Rev. B* **37**, 2770 (1988).
32. K. Murakami, H. Suhara, S. Fujita, and K. Masuda, *Phys. Rev. B* **44**, 3409 (1991).
33. S. J. Pearton and J. Lopata, *App. Phys. Lett.* **59**, 2841 (1991).
34. K. Bergman, M. Stavola, S. J. Pearton, and T. Hayes, *Phys. Rev. B* **38**, 9643 (1988).
35. K. J. Chang and D. J. Chadi, *Phys. Rev. Lett.* **60**, 1422 (1988).
36. P. J. H. Denteneer, C. G. Van de Walle, and S. T. Pantelides, *Phys. Rev. B* **41**, 3885(R) (1990).
37. K. Sato, A. Castaldini, N. Fukata, and A. Cavallini, *Nano Lett.* **12**, 3012 (2012).
38. P. Gupta, V. Colvin, and S. George, *Phys. Rev. B* **37**, 8234 (1988).

Downloaded on 2018-07-20 to IP 207.241.231.81 address. Redistribution subject to ECS terms of use (see ecsdl.org/site/terms_use) unless CC License in place (see abstract).